INORGANIC CHEMISTRY FRONTIERS

RESEARCH ARTICLE

View Article Online
View Journal | View Issue

Cite this: *Inorg. Chem. Front.*, 2025, **12**, 2638

β-$LaTeBO_5$ and $RETeBO_5$ (RE = Y, Gd, Tb): explorations of new optical materials in the RE(III)–Te(IV)–B–O system†

Peng-Fei Chen,[a,b,c] Chun-Li Hu,[a] Ming-Zhi Zhang[a] and Jiang-Gao Mao *[a,b,c]

Exploring new materials and enhancing their optical properties is an endeavor of great significance. Combining different types of optical functional groups, such as borate and tellurite anions, into the same compound can produce a new material of novel structure with enhanced optical performance. In the RE(III)–Te(IV)–B–O system, a borate tellurite, namely, β-$LaTeBO_5$ (β-LTBO) and a series of lanthanide borotellurites, namely, $RETeBO_5$ (RE = Y, Gd, Tb), have been successfully synthesized by using a high-temperature solution method. β-LTBO crystallizes in the space group of $P2_1/c$ (no. 14) and its structure features $[LaTeO_3]_\infty$ layers composed of La^{3+} cations and $[TeO_3]^{2-}$ anions, where these layers are interconnected by $^1[BO_2]_\infty$ chains consisting of $[BO_3]^{3-}$ planar triangles to form a novel 3D structure. $RETeBO_5$ (RE = Gd, Tb, Y) features 0D $[Te_2B_2O_{10}]^{6-}$ clusters in which a central $[Te_2O_6]^{4-}$ dimer connects with two $[BO_3]^{3-}$ groups on both sides of the dimer *via* Te–O–B bridges, and these 0D $[Te_2B_2O_{10}]^{6-}$ clusters are interconnected by lanthanide ions to form the 3D structure. A phase transition from the β phase to the α phase was observed at 700 °C for $LaTeBO_5$ based on DSC and temperature-dependent XRD studies. Excitingly, the birefringence of β-LTBO of 0.134@546 nm is much larger than that of $RETeBO_5$ (RE = Y, Gd) (0.08, 0.074@546 nm), which is the largest in the borate tellurite system. Theoretical calculations indicate that the $^1[BO_2]_\infty$ chains make a considerable contribution to the enhanced birefringence of β-$LaTeBO_5$. Furthermore, the luminescent and magnetic properties of $RETeBO_5$ (RE = Y, Gd, Tb) were also studied. The present study proposes that the investigation of the metal–Te(IV)–B–O system may potentially result in the identification of numerous novel multifunctional materials.

Received 12th December 2024,
Accepted 10th February 2025

DOI: 10.1039/d4qi03203a

rsc.li/frontiers-inorganic

Introduction

Birefringent materials are of great importance in applications such as optical sensors, optical isolators and optoelectronic modulators.[1–6] Despite the availability of commercial birefringent materials, such as α-BaB_2O_4, YVO_4, $CaCO_3$ and MgF_2, their utility in high-end optical applications is constrained by a number of issues.[7] These issues encompass, but are not limited to, the phase transition and facile deliquescence of α-BaB_2O_4, the challenge of growing substantial single crystals of YVO_4 and $CaCO_3$, and the markedly diminished birefringence of MgF_2 observed.[8] Therefore, the development of new high-performance birefringent materials is still a hot research topic.

According to anionic group theory, anionic fundamental building blocks (FBBs) play pivotal roles in the context of optical materials.[9] Anionic FBBs can be primarily classified into two categories: the π-conjugated groups (*e.g.*, $[BO_3]^{3-}$, $[CO_3]^{2-}$, $[NO_3]^-$, $[C_3N_3O_3]^{3-}$) and the non-π-conjugated groups (*e.g.*, $[TeO_3]^{2-}$, $[SeO_3]^{2-}$, $[IO_3]^-$, $[PO_4]^{3-}$, $[SO_4]^{2-}$).[4,10,11] Among these, the $[BO_3]^{3-}$ group has been the focus of researchers' attention due to its great structural diversity and stability, wide transmission range, and large birefringence.[12,13] In 2022, $LiBO_2$ featuring $^1[BO_2]_\infty$ chains, the shortest ultraviolet cutoff edge (164 nm) and the largest birefringence (≥0.168@266 nm) among all of the reported borate-based DUV birefringent materials was described by Pan's group.[14] It can therefore be proposed that highly polymerized $^1[BO_2]_\infty$ chains represent an effective birefringent active unit.[4,12,15] In addition, the $[TeO_3]^{2-}$

[a]*State Key Laboratory of Structural Chemistry, Fujian Institute of Research on the Structure of Matter, Chinese Academy of Sciences, Fuzhou 350002, P. R. China. E-mail: mig@fjism.ac.cn*
[b]*School of Physical Science and Technology, ShanghaiTech University, Shanghai, 201210, P. R. China*
[c]*University of Chinese Academy of Sciences, Beijing, 100049, P. R. China*

†Electronic supplementary information (ESI) available: Crystal data and structure refinements; selected bond lengths and angles; assignment of absorption peaks observed in the IR spectrum; crystal photographs; PXRD patterns; EDS; the coordination environment of La^{3+} ions in β-$LaTeBO_5$; plot of lattice constants for $RETeBO_5$; TG curves; linear optical spectrum; theoretical studies. CCDC 2409211–2409214. For ESI and crystallographic data in CIF or other electronic format see DOI: https://doi.org/10.1039/d4qi03203a

group is a member of another important class of functional groups, which possess sterically active lone-pair electrons, that have susceptibility to second-order Jahn–Teller distortion and substantial microscopic polarizabilities.[16,17] Compared to other non-π-conjugated systems, such as the $[PO_4]^{3-}$ and $[SeO_3]^{2-}$ groups, the $[TeO_3]^{2-}$ group demonstrates significantly greater anisotropy of polarizability, lower phonon energy, and a broader infrared transmission range.[18,19] In 2024, our research group reported $Hg_4(Te_2O_5)(SO_4)$, which features novel $[Hg_4(Te_2O_5)]_\infty$ layers and $[Te_2O_5]^{2-}$ dimers, as well as a large birefringence of 0.542@546 nm.[20]

The combination of these above two types of functional groups into the same compound can lead to new optical materials.[21,22] This is reflected by the borotellurite-like boroselenites, such as $Se_2B_2O_7$,[23] $ASeB_3O_7$ (A = Na, K),[24] $M(B(SeO_3)_3)H_2O$ (M = Al, Ga),[25] *etc*.[21] Among these, $Se_2B_2O_7$ featuring a neutral 3D framework composed of $[B_2O_7]^{8-}$ dimers and $[SeO_3]^{2-}$ units exhibits a moderate SHG efficiency of about 2.2 × KDP. In comparison, the borate–tellurite system is much less explored, mainly due to the possible oxidation of Te(IV) to Te(VI) during high-temperature solid-state reactions.[26–30] This is reflected by $Na_2RE_2TeO_4(BO_3)_2$ (RE = Y, Dy–Lu), whose structures feature a 0D linear $[TeO_4(BO_3)_2]^{8-}$ cluster composed of a $[TeO_6]^{6-}$ unit and two $[BO_3]^{3-}$ groups.[31] To date, only six cases of borotellurites have been reported including $Te(B_4O_8)$,[32] $Te_2B_2O_7$,[33] $A_3BaTeB_7O_{15}$ (A = K, Rb),[34,35] $PbTeB_4O_9$,[36] and $LaTeBO_5$.[37] In addition, a mixed-valence Te (Te^{VI}, Te^{IV}) borate, namely, $Ca_{13}Te_{4.42}O_{15}(BO_3)_4(OH)_3$,[38] has been reported. The only lanthanide borotellurite reported, $LaTeBO_5$ (*Pbca*), features 0D $[Te_2O_4(BO_3)_2]^{6-}$ groups composed of a $[Te_2O_6]^{4-}$ dimer corner-sharing with two $[BO_3]^{3-}$ groups, and has a moderate birefringence value of 0.08@1064 nm.[37] Regrettably, no compounds with birefringence values surpassing 0.1 have been documented within borate–tellurite systems to the best of our current knowledge.

In order to better understand the structure–property relationship of the lanthanide B–Te(IV)–O system and to further enhance the birefringence of borate tellurites, we initiated systematic exploration of RE–B–Te–O system. Our research efforts afforded another form of lanthanum borate tellurite, namely, β-$LaTeBO_5$ (β-LTBO) and a series of lanthanide borotellurites, namely, $RETeBO_5$ (RE = Y, Gd, Tb). The structure of the β-LTBO (space group $P2_1/c$) features a novel 3D network composed of $[LaTeO_3]_\infty$ cationic layers interconnected by $^1[BO_2]_\infty$ anionic chains. Rare earth borate tellurites $RETeBO_5$ (RE = Y, Gd, Tb) are isostructural with α-$LaTeBO_5$ and exhibit 0D $[Te_2B_2O_{10}]^{6-}$ clusters composed of a central $[Te_2O_6]^{4-}$ dimer attached to two $[BO_3]^{3-}$ groups on both sides of the layer *via* a Te–O–B bridge. A phase transition from β-LTBO to α-LTBO was observed at 700 °C. More importantly, β-LTBO exhibits a broad UV transmission range (0.4–6.5 μm) and demonstrates the largest birefringence among borate–tellurite systems, with a value of 0.134@546 nm. In addition, the photoluminescence, radioluminescence and magnetic properties of $RETeBO_5$ (RE = Y, Gd, Tb) were also studied.

Experimental

Reagents and instruments

TeO_2 (Sigma-Aldrich, ≥99.0%), H_3BO_3 (Sigma-Aldrich, ≥99.5%), Na_2CO_3 (Sigma-Aldrich, ≥99.0%), Tb_4O_7 (Sigma-Aldrich, ≥99.0%) and RE_2O_3 (RE = La, Y, Gd, Sigma-Aldrich, ≥99.0%) were used as received without further purification.

A Rigaku Miniflex 600 X-ray diffractometer with graphite-monochromated Cu-Kα radiation in the 2θ range of 10–70° was used to record powder X-ray diffraction (PXRD) patterns of the samples. Thermogravimetry (TG) and differential scanning calorimetry (DSC) studies were carried out on a NETZCH STA 449F3 thermal analyzer in the temperature ranges of 30 to 1000 °C and 30 to 800 °C with a heating rate of 10 °C min^{-1} under a nitrogen atmosphere. Infrared (IR) spectra were recorded on a Nicolet Magna 750 FT-IR spectrometer with air as background in the range of 4000–400 cm^{-1} and at a resolution of 2 cm^{-1}. A PerkinElmer Lambda 950 ultraviolet-visible-near infrared (UV-vis-NIR) spectrophotometer was used to acquire UV-vis-NIR spectra in the wavelength range of 190 to 2500 nm with $BaSO_4$ as the 100% reflectance reference. A field emission scanning electron microscope (FESEM, JSM6700F) with an energy dispersive X-ray spectroscope (Oxford INCA) was used to perform microprobe elemental analyses. Photoluminescence studies were performed on an Edinburgh FLS980 fluorescence spectrometer. Radioluminescence (RL) emission spectra were recorded using an X-ray source (12 W, TUB00146-W06, Magpro) and a fiber-optic spectrometer (PG2000 Pro, Ideaoptics, China). The light yield, defined as the ratio of the number of produced photons to the energy of X-rays (MeV), was assessed by a relative method where a commercial $Bi_4Ge_3O_{12}$ (BGO) single crystal (8000 ph MeV^{-1}) scintillator was used as a reference. Magnetic susceptibility measurements on polycrystalline samples were performed with a PPMS-9 T magnetometer at a field of 1000 Oe in the temperature range of 2–300 K. The birefringence values were measured by using a polarizing microscope (Nikon Eclipse LV100N POL) equipped with a Berek compensator. The wavelength of the light source was 546 nm. Before scanning, small and transparent crystals were chosen to be measured, in order to improve the accuracy of the birefringence. The thickness of selected crystals was measured on the polarizing microscope.

Syntheses

Single crystals of β-$LaTeBO_5$ and $RETeBO_5$ (RE = Y, Gd, Tb) were synthesized by high-temperature solution reactions utilizing Na_2CO_3 as flux. A mixture of 1 : 3 molar ratio TeO_2 and H_3BO_3 was achieved through a ball milling process, comprising 30 minutes of forward and 30 minutes of reverse rotation at 1200 rpm. Subsequently, the resulting mixture (0.7 g), RE_2O_3 (RE = La, Y, Gd) or Tb_4O_7, (0.4 mmol) and Na_2CO_3 (1 mmol) were ground evenly and added to a ∅ 2 × 2 cm platinum crucible. The platinum crucible was heated to 820 °C over the course of one day and held at this temperature for a further three days. It was then cooled to 300 °C over the course of ten days, after which the furnace was switched off. After

washing the products with deionized water and ethanol, colourless sheet-shaped crystal of β-$LaTeBO_5$ and block-shaped crystals of $RETeBO_5$ (RE = Y, Gd, Tb) were obtained (Fig. S1†) in the yields of approximately 10% in terms of the RE element. The purities of the samples were verified by powder X-ray diffraction (PXRD) analysis (Fig. S2†). The EDS analysis demonstrates the presence of the RE, Te, B and O elements (Fig. S3†).

Single-crystal structure determination

Single-crystal X-ray diffraction data of β-$LaTeBO_5$ and $RETeBO_5$ (RE = Y, Gd, Tb) were acquired using a Rigaku Oxford Diffraction SuperNova CCD diffractometer with a 293/150 K (Mo) X-ray source (λ = 0.71073 Å). Data reductions were performed using CrysAlisPro and absorption corrections were applied on the basis of a multi-scan approach. All structures were solved with the ShelXT 2018/2 solution program[39] using direct methods and by using Olex2-1.5[40] as the graphical interface. The models were refined with ShelXL 2018/3[41] using full-matrix least-squares minimization on F^2. All of the non-hydrogen atoms were refined with anisotropic thermal parameters. By using the program PLATON,[42] a check for possible missing symmetries in the four structures was performed, but none were found. Crystal data and structure refinements for the four compounds are listed in Table S1,† and selected bond lengths are reported in Tables S2 and S3.†

Computational description

Theoretical calculations for the electronic structure and optical properties of β-$LaTeBO_5$, $YTeBO_5$ and $GdTeBO_5$ were performed using the first-principles plane wave pseudopotential method of density functional theory (DFT), which was implemented by the total energy code CASTEP.[43,44] The DFT calculations employed the GGA-PBE exchange–correlation function.[45] The interactions between the ionic nuclei and the electrons were described by the norm-conserving pseudopotential.[46] La $5d^16s^2$, Y $4d^15s^2$, Gd $5s^25p^64f^75d^16s^2$, Te $5s^25p^4$, B $2s^22p^1$ and O $2s^22p^4$ were considered as valence electrons. The numbers of plane waves contained in the basis set of all compounds were determined with cutoff energy values of 750 eV (La, Y) and 820 eV (Gd) and Monkhorst–Pack *k*-point sampling of 2 × 3 × 3 (La) and 2 × 4 × 2 (Y, Gd) being used for numerical integration in the Brillouin zone. The default values of the CASTEP code were applied for the other calculation parameters and convergence criteria used in the calculations. Gaussian 09[47] was mainly employed to calculate the polarizability anisotropy (δ) of the microscopic units. Density functional theory was selected as the calculation method, and 6-31G/LANL2DZ was used as the basis set. Multiwfn[48] was used to extract the polarizability anisotropy in the Gaussian 09 output file.

Results and discussion

Crystal structure descriptions

β-$LaTeBO_5$ (β-LTBO) is a borate-tellurite mixed-anion compound, which crystallizes in the centrosymmetric monoclinic space group $P2_1/c$ (no. 14). Its structure features a novel 3D network composed of $[LaTeO_3]_\infty$ layers interconnected by $^1[BO_2]_\infty$ chains (Fig. 1a). The asymmetric unit of β-LTBO comprises two La atoms, two Te atoms, two B atoms and ten O atoms, which occupy the 4*e* Wyckoff position. Both Te^{4+} ions are in three-coordinated $[TeO_3]^{2-}$ trigonal pyramidal geometry while both boron atoms are in $[BO_3]^{3-}$ planar triangular geometry. The Te–O bond distances and O–Te–O bond angles are 1.850(3) Å to 1.866(3) Å and 91.90(14)° to 103.03(14)°, respectively. The B–O bond lengths are in the range of 1.305(6)–1.396 (6) Å and the O–B–O angles fall within 114.4(4)–128.4(4)°. The two La^{3+} cations in the asymmetric unit are coordinated by nine O atoms, forming an $[LaO_9]^{15-}$ triangular prism (TTP) structure with La–O bond distances ranging from 2.429(3) Å to 2.929(3) Å (Fig. S4a and S4b†). These bond lengths and angles are in close agreement with those reported in the literature.[37,49–52] The calculated bond valence sums for La^{3+}, Te^{4+}, B^{3+} and O^{2-} of 3.201–3.228, 4.116–4.123, 3.044–3.077 and 1.793–2.238 (Table S4†), respectively, correspond to the expected oxidation states.

The interconnection of La(1) atoms and $Te(1)O_3$ groups results in a 2D $[La(1)Te(1)O_3]_\infty$ layer (Fig. 1b), as does the La(2)

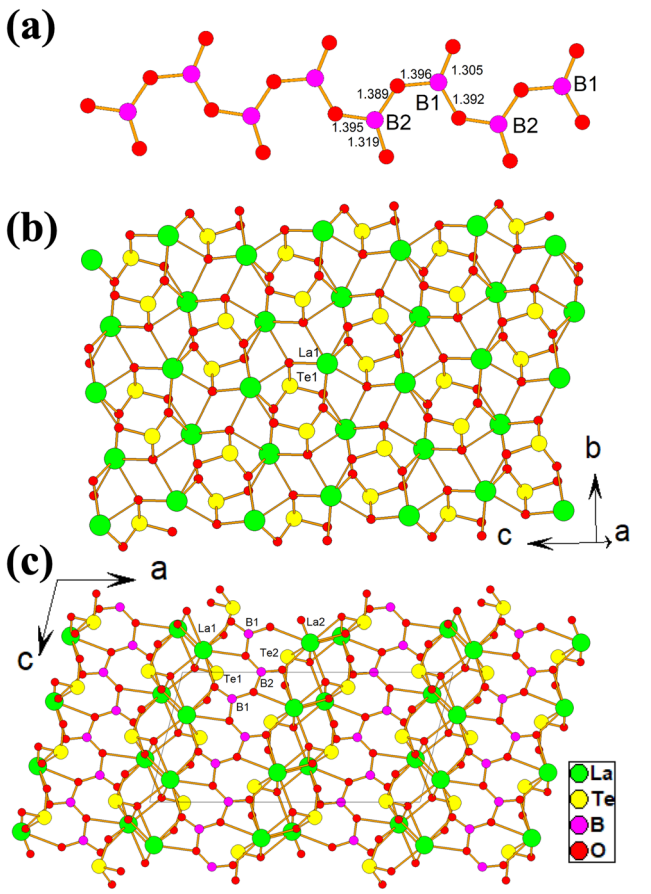

Fig. 1 Crystal structure of β-$LaTeBO_5$: (a) a $^1[BO_2]_\infty$ chain linked by $[BO_3]^{3-}$ units; (b) a 2D $[LaTeO_3]_\infty$ layer; (c) the 3D network structure viewed along the *b*-axis.

atoms and Te(2)O_3 groups. The interconnection of B(1)O_3 and B(2)O_3 groups *via* corner-sharing leads to $^1[BO_2]_\infty$ chains (Fig. 1a). The two different $[LaTeO_3]_\infty$ layers are interconnected by $^1[BO_2]_\infty$ chains *via* B–O–La bridges and formed into a 3D network structure (Fig. 1c). In terms of connectivity, the layer of β-LTBO can be described as a neutral framework comprising the following units: $\{2[TeO_{1/2}O_{1/3}O_{1/4}]2[BO_{3/3}]2[LaO_{1/2}O_{5/3}O_{3/4}]\}$. In accordance with the dipole–dipole interaction model, the polymerization of $[BO_3]^{3-}$ planar triangles within the same plane has the potential to enhance the average anisotropy of polarizabilities. It can be reasonably deduced that the highly polymerized $^1[BO_2]_\infty$ chains will have larger average anisotropic polarizabilities than those of isolated $[BO_3]^{3-}$ groups, which will in turn result in a larger birefringence.

$RETeBO_5$ (RE = Y, Gd, Tb) are isomorphic with the borotellurite α-$LaTeBO_5$ previously reported and crystallize in the orthorhombic crystal system with the centrosymmetric space group *Pbca* (no. 61).[37] $GdTeBO_5$ will be used here as a representative example to illustrate the general characteristics of this family of compounds. Two $[TeO_4]^{4-}$ groups form a $[Te_2O_6]^{4-}$ dimer *via* edge-sharing, and the two $[BO_3]^{3-}$ groups are attached on both sides of the $[Te_2O_6]^{4-}$ groups through corner-sharing, thereby forming the 0D $[Te_2B_2O_{10}]^{6-}$ anion cluster (Fig. 2a). Each 0D $[Te_2B_2O_{10}]^{6-}$ cluster is connected to ten Gd^{3+} ions (Fig. 2a), thereby forming a 3D network structure

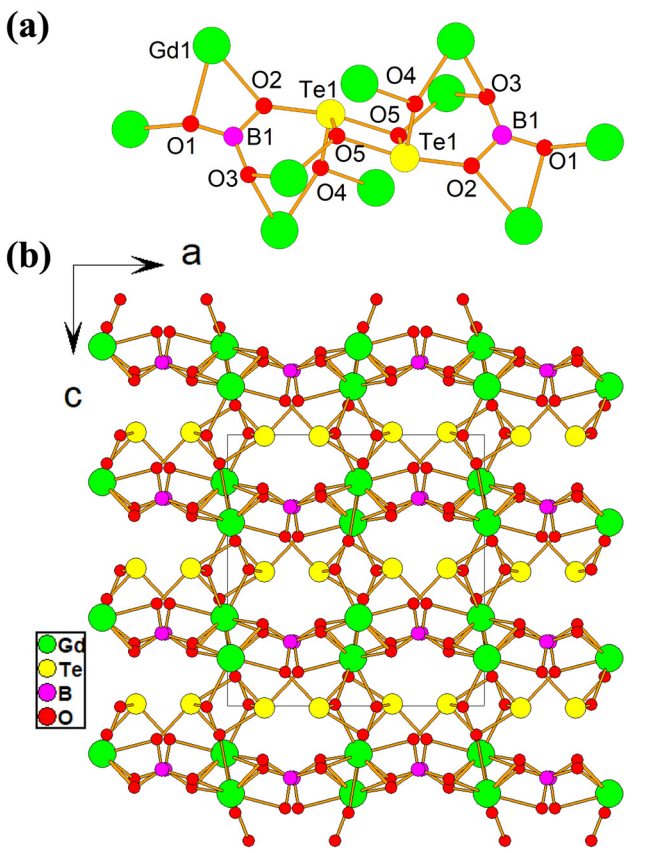

Fig. 2 Crystal structure of $GdTeBO_5$: (a) a 0D $[Te_2B_2O_{10}]^{6-}$ cluster; (b) the 3D network structure viewed along the *b*-axis.

(Fig. 2b). The bond lengths of B–O, Te–O and RE–O in $RETeBO_5$ (Table S3†) are in the range of 1.343(7)–1.419(8) Å, 1.868(5)–2.181(5) Å and 2.307(4)–2.501(4) Å, respectively, which are close to those observed in α-LTBO. As illustrated in Fig. S5,† a reduction in the radius of rare earth ions in eight-fold coordination was observed, resulting in a linear relationship between the lattice parameters (which includes the *a*, *b*, *c*, and *V* parameters) and the changes in lanthanide ionic radius.

Structural comparisons

It is interesting to compare β-$LaTeBO_5$ and $RETeBO_5$ (RE = Y, Gd, Tb) with reported borotellurites. Among the six examples of borotellurites that have been reported, the ternary compounds TeB_4O_8 and $Te_2B_2O_7$ were synthesized in a high-temperature and high-pressure environment.[32,33] TeB_4O_8 (*C*2/*c*) features a 3D network composed of borate double layers of corner-sharing $[BO_4]^{5-}$ tetrahedra, which are seesaw-shaped coordinated with Te^{4+} ions,[26] whereas the polar $Te_2B_2O_7$ (*Pna*2$_1$) exhibits a different 3D network composed of 1D chains of corner-sharing $[BO_4]^{5-}$ groups, $[B_2O_7]^{8-}$ dimers, 1D chains of corner-sharing $[TeO_4]^{4-}$ groups, and $[Te_2O_6]^{4-}$ dimers composed of two edge-sharing $[TeO_4]^{4-}$ groups. $A_3BaTeB_7O_{15}$ (A = K, Rb) and $PbTeB_4O_9$ display two different layered structures. $A_3BaTeB_7O_{15}$ (A = K, Rb) exhibits a $[B_7O_{13}]^{5-}$ double layer with 1D tunnels of eight member-rings where the$[TeO_3]^{2-}$ motifs are attached on both sides of the borate double layer *via* corner-sharing, while $PbTeB_4O_9$ features a $[B_4O_8]_\infty$ layer with $[TeO_3]^{2-}$ groups grafted to the side of the borate layer by forming three-membered rings.[34–36] 0D $[Te_2B_2O_{10}]^{6-}$ borotellurite clusters were found in α-$LaTeBO_5$ [37] and $RETeBO_5$ (RE = Y, Gd, Tb). It is of note that the introduction of charge-balance cations normally reduces the dimensionality of the borotellurite anions. In the case of borate tellurite, there is only one mixed-valence $Ca_{13}Te_{4.42}O_{15}(BO_3)_4(OH)_3$. It consists of separate $[BO_3]^{3-}$, $[TeO_4]^{4-}$ and $[Te_3O_6]^{2+}$ trimers forming the anionic backbone.[38] In contrast, β-LTBO consists of $[BO_3]^{3-}$ groups in a co-corner to form a $^1[BO_2]_\infty$ chain, which further connects the La–Te–O layers to form a 3D structure.

It is also instructive to compare the structures of our lanthanide B–Te–O compounds with those of $La(TeO_3)(NO_3)$ and $AKTeO_2(CO_3)$ (A = Li, Na).[53,54] $La(TeO_3)(NO_3)$ has a La–Te–O layer similar to that of β-LTBO, but the $[NO_3]^-$ groups are isolated with respect to each other. $AKTeO_2(CO_3)$ (A = Li, Na) structures have similar 0D $[Te_2C_2O_{10}]^{4-}$ clusters, similar to those of $[Te_2B_2O_{10}]^{6-}$ in $RETeBO_5$ (RE = Y, Gd, Tb). The replacement of the two $[BO_3]^{3-}$ groups by $[CO_3]^{2-}$ groups results in different negative charges for the clusters.

Thermal analysis and phase transformations

The thermal stability of β-LTBO and $RETeBO_5$ (RE = Y, Gd, Tb) was analyzed with decomposition temperatures of 860, 870, 884, and 882 °C, respectively (Fig. S6†), which are similar to that of α-LTBO (887 °C). The DSC curve of β-LTBO was further investigated below the decomposition temperature (Fig. 3a), and an endothermic peak appeared at 736 °C, whereas the TG curves remained unchanged, suggesting a possible phase transition.

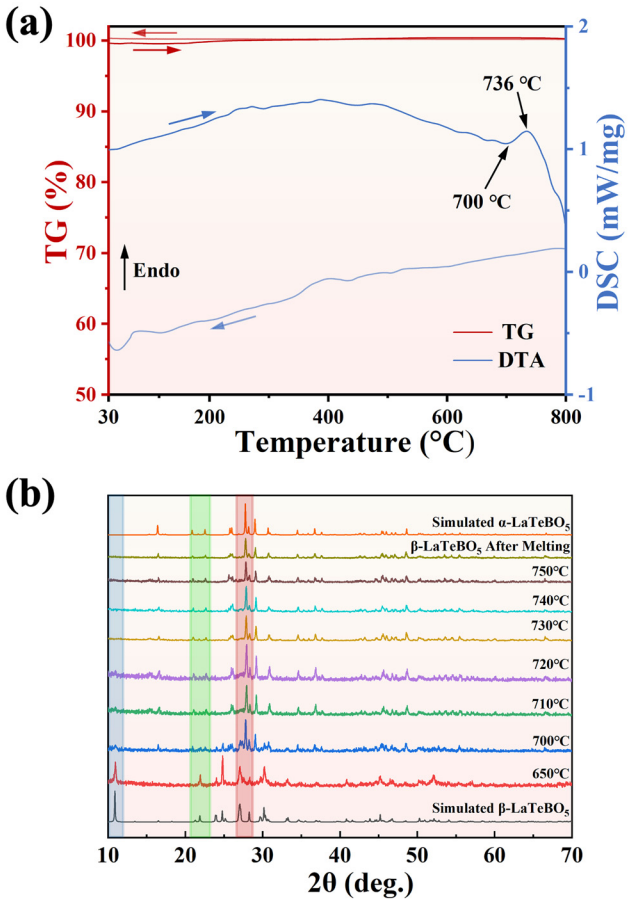

Fig. 3 (a) TG and DSC curves of β-$LaTeBO_5$. (b) Simulated and experimental PXRD patterns of $LaTeBO_5$ at different temperatures.

In order to ascertain whether a phase transition occurs, β-LTBO was heated to 650, 700, 710, 720, 730, 740 and 750 °C and maintained at each temperature for a period of one day. The resultant samples were subjected to X-ray diffraction (XRD) analyses (Fig. 3b). At 650 °C, the peaks at 11° (blue area) and 27° (red area) correspond to the β phase, while the peak at 26° (green area) is attributed to the α phase. This suggests that a portion of the β phase has undergone a transformation into the α phase. When the temperature is raised to 700 °C, the peak at 11° disappears, while the peak at 41° (red area) remains, proving that the phase transition is not yet complete. Upon reaching 730 °C, the product undergoes a complete transformation into a new phase, corresponding to the inflection point at 700 °C and the peak at 736 °C in the DSC curve. The XRD patterns of the melted samples are consistent with those of α-LTBO, indicating that β-LTBO has the phase transition.

Spectral measurements

The infrared and UV-vis-NIR diffuse reflectance spectra of β-LTBO and $RETeBO_5$ (RE = Y, Gd, Tb) are presented in Fig. S7a and S7b.† All of these compounds display a broad infrared transmission spectrum, exhibiting complete transmissivity within the range of 0.4–6.5 μm. The pronounced absorption bands observed at 1503, 1319–1328, and 1170–1181 cm^{-1} can be ascribed to the asymmetric stretching of the $[BO_3]^{3-}$ groups. The peaks at 916–943 cm^{-1} can be attributed to the symmetric stretching vibration of B–O in the $[BO_3]^{3-}$ units. The bands associated with the $[BO_3]^{3-}$ bending modes are located at 582–592 cm^{-1}. The absorption peaks at 705–653 and 470–445 cm^{-1} are attributed to the doubly degenerate antisymmetric stretching and symmetric stretching vibration modes of the $[TeO_3]^{2-}$ units. The IR spectra confirm the existence of the B–O and Te–O units (Table S4†), and their absorption bands are consistent with those previously reported for borates and tellurites in the literature.[34–37] β-LTBO and $RETeBO_5$ (RE = Y, Gd, Tb) exhibit their ultraviolet cutoff edge at 256, 240, 244, and 259 nm, and have estimated experimental band gap values of 4.08, 4.46, 4.42, and 3.74 eV according to the Kubelka–Munk function, respectively (Fig. S7c†), which are analogous to those observed for α-LTBO (246 nm, 4.20 eV).[37]

Photoluminescence (PL) and radioluminescence (RL)

Irradiation of the four crystals under a UV lamp at 365 nm revealed that only $TbTeBO_5$ exhibited robust luminescence characteristics. The solid-state photoluminescence (PL) spectra of $TbTeBO_5$ were investigated at room temperature (Fig. 4a). The emission of $TbTeBO_5$ is primarily attributable to transitions between the $^5D_4$ state and the ^7F_J (J = 6, 5, 4, 3) states. The $^5D_4 \rightarrow {}^7F_6$ transition, occurring at a wavelength of approximately 480–500 nm, exhibits multiple sub-peaks, while the $^5D_4 \rightarrow {}^7F_5$, $^7F_4$, and $^7F_3$ transitions generate fine-structure peaks at wavelengths of approximately 540–550 nm, 580–590 nm, and 610–630 nm, respectively. This splitting is caused by the strong influence of the crystal field on Tb^{3+} energy levels and the

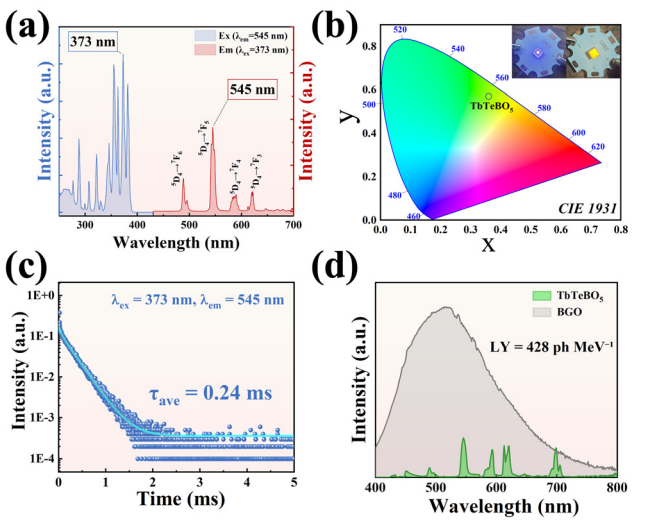

Fig. 4 (a) Steady-state PL excitation (left) and PL emission (right) spectra of $TbTeBO_5$ at RT. (b) The corresponding CIE coordinate and the corresponding photoluminescence image (inset). (c) PL decay of $TbTeBO_5$ by monitoring the emission at 545 nm (λ_{ex} = 373 nm). (d) Comparison of the radioluminescence spectra of BGO and $TbTeBO_5$.

asymmetric coordination environment around the ion.[55,56] The strongest emission band is at 545 nm, and the chromaticity coordinate is (0.36, 0.57), which corresponds to green light (Fig. 4b). The decay curve obtained from the polycrystalline sample of $TbTeBO_5$ upon 373 nm near ultraviolet excitation indicates that the effective lifetime of $TbTeBO_5$ is 0.24 ms for 545 nm emission (Fig. 4c). Furthermore, the photoluminescence quantum yields (PLQYs) were measured as high as 44.06%, indicating that $TbTeBO_5$ may be a promising luminescent material for green-light emission.

The possible existence of radioluminescence (RL) in $TbTeBO_5$ was investigated after confirming its PL properties. $TbTeBO_5$ produced RL with the same emission bands related to PL, as reported above (Fig. 4d). The integral emission of $TbTeBO_5$ was compared with that of the commercial scintillator BGO, yielding a relative luminosity of 5.4% at room temperature. In accordance with the aforementioned scintillator, the light yield (LY), defined as the ratio of the number of produced photons to the energy of the X-rays, was 428 ph MeV^{-1} in $TbTeBO_5$ calculated with respect to BGO.[57]

Birefringence

The birefringence of β-LTBO, $YTeBO_5$ and $GdTeBO_5$ was determined by employing a cross-polarizing microscope. The birefringence of the crystal can be calculated using the following formula: $R = \Delta n \times d$, where R, Δn and d represent retardation, birefringence and thickness, respectively. As illustrated in Fig. S8,† crystal thicknesses are approximately 4.84, 109.74 and 51.62 μm, respectively. According to the chart of Michal Levy, the respective retardation values are approximately 615, 8461 and 3625 nm. Accordingly, the birefringence values of 0.127, 0.077 and 0.070@546 nm are derived from the aforementioned formula, which are almost equal to the values from theoretical calculations. It is worth noting that the birefringence of β-LTBO is close to that of borates containing $^1[BO_2]_\infty$ chains, such as $LiBO_2$ (0.126@1064 nm),[14] $Ca(BO_2)_2$ (0.124@1064 nm),[58] and $Li_{0.5}Na_{0.5}AlB_2O_4F_2$ (LNABF) (0.108@546 nm).[15] It can also be concluded that the birefringence of β-LTBO is the largest among those of compounds in B–Te–O and other systems composed of the Te element and π-conjugated planar triangle groups (Fig. 5). More significantly, a comparison is conducted between β-LTBO and commercially available birefringent crystals, such as YVO_4 and α-BaB_2O_4. At 546 nm, the birefringence of β-LTBO is 0.65 times that of YVO_4 and 1.10 times that of α-BaB_2O_4. Additionally, β-LTBO exhibits excellent stability in air and possesses a wide transmission range from 0.4 to 6.5 μm, making β-LTBO a promising candidate for commercial birefringent materials.

Magnetic properties

We measured the temperature dependence of the magnetic susceptibility (χ) of our samples in the temperature range of 2 K to 300 K under an applied magnetic field H = 1000 Oe. For $GdTeBO_5$, $\chi(T)$ increases monotonically upon cooling, showing typical paramagnetic behavior in the range of 2–300 K (Fig. 6a). This good linear behavior can be observed in the

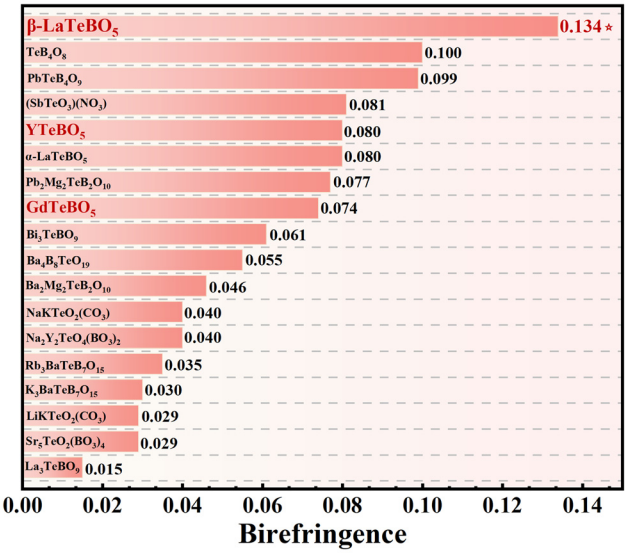

Fig. 5 Birefringence values of the reported compounds containing Te and π-conjugated group systems.

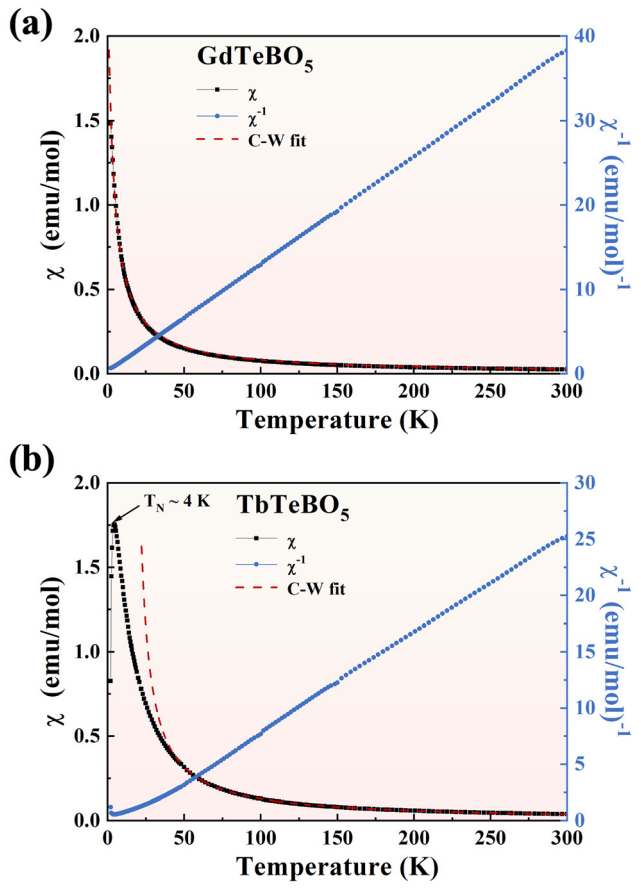

Fig. 6 Temperature-dependent magnetic susceptibility (χ) (black squares) and inverse magnetic susceptibility (χ^{-1}) (blue balls) for $GdTeBO_5$ (a) and $TbTeBO_5$ (b). The red dashed lines are corresponding fits using the standard Curie–Weiss (C–W) law. The AFM transition temperature of $TbTeBO_5$ is marked in (b).

corresponding plot of the temperature-dependent inverse susceptibility (χ^{-1}) over the whole temperature range. The behavior of $\chi(T)$ can be well-fitted by a standard Curie–Weiss law ($\chi = C/(T - \theta_{C-W})$), which yields a small negative Curie–Weiss temperature ($\theta_{C-W} = -2.16$ K), suggesting the existence of mainly weak antiferromagnetic exchange interactions between magnetic Gd ions in this compound. The fitted effective magnetic moment μ_{eff} is about 7.93μ_B per Gd ion. This value is in excellent agreement with the magnetic moment of μ_{calc} = 7.94μ_B for Gd^{3+} (with $J = S = 7/2$) calculated using Hund's rules. For $TbTeBO_5$, $\chi(T)$ increases upon cooling at high temperature, while below 4 K, it drops rapidly, suggesting an antiferromagnetic (AFM) transition (Fig. 6b). The corresponding Néel temperature (T_N) is close to 4 K. The corresponding good linearity for $\chi^{-1}(T)$ is well maintained in the high-temperature paramagnetic range. The value of $\chi(T)$ is well-fitted by the C–W formula in the high-temperature range (above 30 K), yielding a positive θ_{C-W} (15.38 K), suggesting the presence overall of mainly ferromagnetic exchange interactions between neighboring Tb ions in this compound. The fitted effective magnetic moment μ_{eff} is about 9.35μ_B. This value is very close to that of Tb^{3+} (μ_{calc} = 9.72μ_B with J = 6 and g_J = 3/2), rather than that of Tb^{4+} (μ_{calc} = 7.94μ_B with $J = S$ = 7/2 and g_J = 2), confirming trivalent Tb ions as the majority in our compound.[52,59,60]

Theoretical studies

Theoretical calculations were performed using density functional theory (DFT) methods. The band structure calculations revealed that β-LTBO is an indirect band gap compound with a gap of 3.37 eV (Fig. S9a†), while $YTeBO_5$ and $GdTeBO_5$ are direct band gap compounds with gaps of 3.66 and 3.69 eV (Fig. S9b and S9c†). The experimental band gaps of three compounds are slightly lower than the measured values due to the limitations of the GGA functional. Subsequently, the optical property calculations were verified by employing the scissor correction of 0.71 (La), 0.80 (Y) and 0.73 (Gd). As illustrated in Fig. S10,† the density of states (DOS) of β-LTBO, $YTeBO_5$ and $GdTeBO_5$ are analogous in terms of proximity to the Fermi level. The top-most valence band, situated at −10 to 0 eV, is predominantly characterized by the participation of O-2p, Te-5s5p and B-2p orbitals. In addition, Gd displays a strong spin-polarized characteristic and Gd-4f orbitals are involved in the formation of the valence band. The bottom of the conduction band, located at 0 to 10 eV, is primarily attributed to the involvement of Te-5p, La-5d/Y-4d/Gd-5d4f and B-2p orbitals. The density of states (DOS) of B, Te, RE and O exhibit a high degree of overlap in the B–O, Te–O and RE–O bonds. The optical properties of β-LTBO, $YTeBO_5$ and $GdTeBO_5$ were calculated. The results demonstrate that the birefringence (Δn) values of β-LTBO are 0.134@546 nm and 0.118@1064 nm (Fig. 7a), which are the maximum values among compounds containing Te(IV) and π-conjugated group systems (Table S5†). Additionally, the birefringence (Δn) values of $YTeBO_5$ and $GdTeBO_5$ are 0.080 and 0.074@546 nm, which are similar to that of α-LTBO (0.083@532 nm) (Fig. 7b and c).

The origin of the large birefringence in β-LTBO was further analyzed. From the perspective of group arrangement, the dihedral angles between the $B(1)O_3$ and $B(2)O_3$ motifs on the $^1[BO_2]_\infty$ chain are 9.8° and 17.7°. The chain is completely coplanar and oriented in the same direction with large structural anisotropy, which is beneficial to large birefringence. From the perspective of its electronic structure, the electron

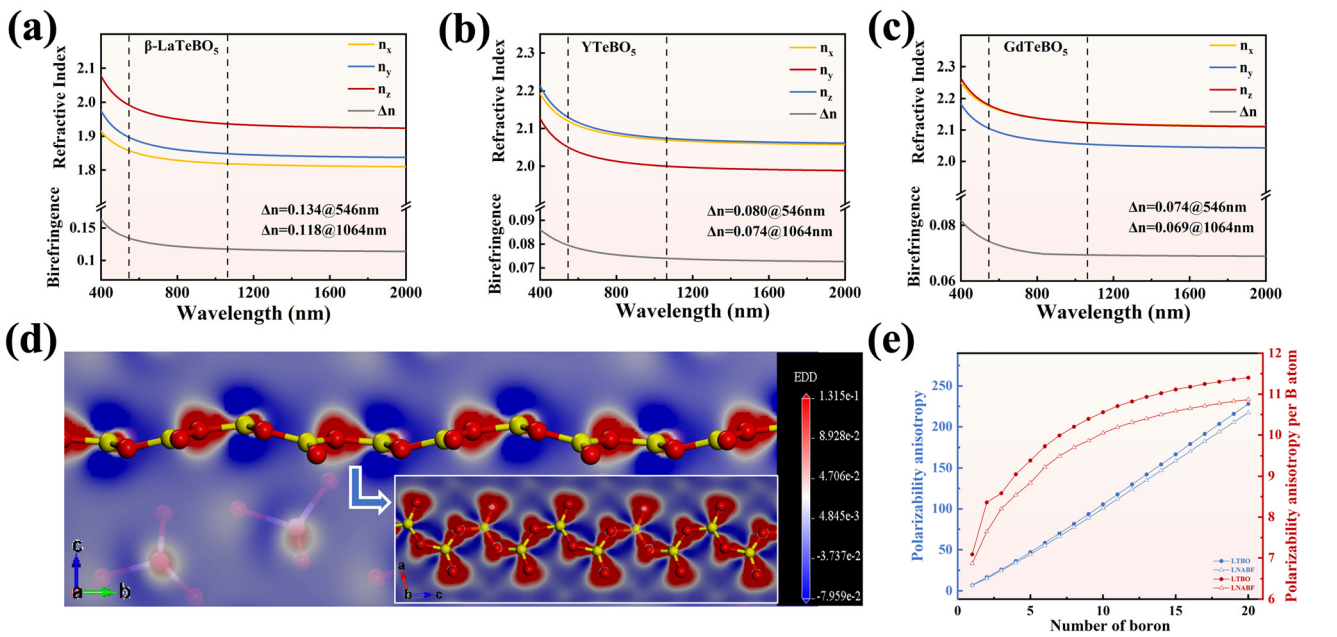

Fig. 7 Calculated refractive indices and birefringence values for β-$LaTeBO_5$ (a), $YTeBO_5$ (b), and $GdTeBO_5$ (c). Electron density difference maps of the $^1[BO_2]_\infty$ chain in β-$LaTeBO_5$ (d). Polarizability anisotropy and permutation contribution rate in β-$LaTeBO_5$ and $Li_{0.5}Na_{0.5}AlB_2O_4F_2$ depending on the numbers of boron atoms in B_nO_{2n+1} (n = 1, 2, ..., 20) (e).

density difference (EDD) map of β-LTBO was calculated (Fig. 7d). There is a continuous accumulation of electron density outside the $^1[BO_2]_\infty$ plane, extending across the entire group plane, suggesting highly delocalized π electrons in the vertical direction. The cross-sectional view in this direction vividly revels the delocalized nature of the π electron cloud, as indicated by the red-shaded area along the $^1[BO_2]_\infty$ chain. In contrast, the localized distribution of the σ bond along the B–O direction within the plane highlights the localized electronic property of the σ bond. Thus, the charge density forms a large contrast between the in-plane and out-of-plane regions, resulting in huge anisotropy. Furthermore, we analyzed the EDD diagram for the $[TeO_3]^{2-}$ group. As illustrated in Fig. S11,† it is evident that the lone-pair electrons of the $[TeO_3]^{2-}$ group are aligned along the *c*-axis, while the π-conjugated delocalization direction of the $^1[BO_2]_\infty$ chain is oriented along the *b*-axis. Unfortunately, these two directions are nearly perpendicular to each other, which does not facilitate favorable synergistic effects on the birefringence performance. Consequently, the birefringence of β-LTBO is primarily attributed to the $^1[BO_2]_\infty$ chain.

In order to show the effect of $[BO_3]^{3-}$ group aggregation into the $^1[BO_2]_\infty$ chain on birefringence, we calculated the polarizability anisotropy values of B_nO_{2n+1} (n = 1, 2, ..., 20), namely $\delta_{\text{total}(n(B))}$. The results show that $\delta_{\text{total}(n(B))}$ increases linearly with chain elongation (Fig. 7e). Compared with the discrete $[BO_3]^{3-}$, the promotion effect of π-conjugated delocalization on the $^1[BO_2]_\infty$ chain can be expressed by $\delta_{\text{total}(n(B))}/(n(B) \times \delta_{B(n=1)})$, which is denoted the permutation contribution rate (PCR). As shown in the Fig. 7e, the PCR increases steadily with the increase of the number of $[BO_3]^{3-}$ groups until it converges and reaches a plateau value of 1.61. The δ_{total} is much larger than the sum of $\delta_{B(n=1)}$, indicating that the π-conjugated delocalization effect can maximize the superposition of FBBs in the chain direction, thereby maximizing the birefringence. Compared with LANBF, which has similar $^1[BO_2]_\infty$ chains, the $\delta_{\text{total}(n(B))}$ and PCR values of β-LTBO are better than those of LANBF. This indicates that the π-conjugated electron delocalization of the $^1[BO_2]_\infty$ chain in β-LTBO is improved, and optimal coplanarity in chains of the same type is exhibited, which further leads to the increase of birefringence.

Conclusions

In summary, β-$LaTeBO_5$ and $RETeBO_5$ (RE = Y, Gd, Tb) have been successfully synthesized by using a high-temperature solution method. β-$LaTeBO_5$ comprises two homozygous $[TeLaO_3]_\infty$ layers interconnected by a $^1[BO_2]_\infty$ chain into a 3D structure. $RETeBO_5$ (RE = Y, Gd, Tb) exhibits 0D $[Te_2B_2O_{10}]^{6-}$ clusters bridged by lanthanide ions into a different 3D structure. A phase transition from the β phase to the α phase at 700 °C was observed for $LaTeBO_5$. The birefringence of β-LTBO of 0.134@546 nm is much larger than that of $RETeBO_5$ (RE = Y, Gd, Tb), which is due to the $^1[BO_2]_\infty$ chains of $[BO_3]^{3-}$ groups in β-$LaTeBO_5$. Additionally, β-LTBO demonstrates the largest birefringence within the borate–tellurite system. $TbTeBO_5$ emits green light with a long lifetime of 0.24 ms. This work demonstrates that explorations in metal–Te(IV)–B–O systems may lead to the discovery of numerous novel multifunctional materials.

Author contributions

Peng-Fei Chen: investigation, validation and writing – original draft; Chun-Li Hu: formal analysis; Ming-Zhi Zhang: investigation; Jiang-Gao Mao: conceptualization, supervision, writing – review & editing and funding acquisition.

Data availability

The data that support the findings of this study are available in the ESI† of this article.

Conflicts of interest

There are no conflicts to declare.

Acknowledgements

This work was supported by the National Natural Science Foundation of China (22031009, 22375201 and 21921001), the Natural Science Foundation of Fujian Province (2023J01216) and the Self-deployment Project Research Program of Haixi Institutes, Chinese Academy of Sciences (CXZX-2022-GH06). We thank Li Zhao, Chen-Liang Li and Hao-Yu Zhang from Fujian Institute of Research on the Structure of Matter, CAS, for measuring the magnetic properties, and recording PL and RL spectra.

References

1 P. F. Li, C. L. Hu, J. G. Mao and F. Kong, Old tree blossoms anew: Research progress on the structures and optical properties of ultraviolet selenites, *Coord. Chem. Rev.*, 2024, **517**, 216000.
2 G. Liu, Advances in the theoretical understanding of photon upconversion in rare-earth activated nanophosphors, *Chem. Soc. Rev.*, 2015, **44**, 1635–1652.
3 M. Mutailipu, K. R. Poeppelmeier and S. Pan, Borates: A Rich Source for Optical Materials, *Chem. Rev.*, 2021, **121**, 1130–1202.
4 A. Tudi, S. J. Han, Z. H. Yang and S. L. Pan, Potential optical functional crystals with large birefringence: Recent advances and future prospects, *Coord. Chem. Rev.*, 2022, **459**, 214380.
5 Q. Z. Zhang, R. An, Z. H. Yang, X. F. Long, S. L. Pan and Y. Yang, Review on birefringence in borates based on bire-

fringence-active functional groups and arrangements, *Sci. China: Chem.*, 2024, **67**, 2155–2170.
6 Y. Q. Zhao, L. M. Zhu, Y. Q. Li, X. J. Kuang, J. H. Luo and S. E. Zhao, Design and synthesis of anisotropic crystals with π-conjugated rings toward giant birefringence, *Mater. Chem. Front.*, 2023, **7**, 3986–3993.
7 S. Han, A. Tudi, W. Zhang, X. Hou, Z. Yang and S. Pan, Recent Development of SnII, SbIII-based Birefringent Material: Crystal Chemistry and Investigation of Birefringence, *Angew. Chem., Int. Ed.*, 2023, **62**, e202302025.
8 P. F. Li, C. L. Hu, J. G. Mao and F. Kong, $Pb_2(SeO_3)(SiF_6)$: the first selenite fluorosilicate with a wide bandgap and large birefringence achieved through perfluorinated group modification, *Chem. Sci.*, 2024, **15**, 7104–7110.
9 C.-T. Chen, An Ionic Grouping Theory of the Electro-Optical and Non-Linear Optical Effects of Crystals (I), *Acta Phys. Sin.*, 1976, **25**, 146–161.
10 X. Dong, L. Huang and G. Zou, Rational Design and Controlled Synthesis of High-Performance Inorganic Short-Wave UV Nonlinear Optical Materials, *Acc. Chem. Res.*, 2025, **58**, 150–162.
11 Y. Tian, W. Zeng, X. Dong, L. Huang, Y. Zhou, H. Zeng, Z. Lin and G. Zou, Enhanced UV Nonlinear Optical Properties in Layered Germanous Phosphites through Functional Group Sequential Construction, *Angew. Chem., Int. Ed.*, 2024, **63**, e202409093.
12 C. Tu, A. Tudi, W. Jin, C. Xie and Z. Yang, $CaBO_2F$: A novel deep-UV structural template with high nonlinear optical performance induced by electron delocalization, *Sci. China Mater.*, 2022, **66**, 1197–1204.
13 S. Wang, N. Ye, W. Li and D. Zhao, Alkaline Beryllium Borate $NaBeB_3O_6$ and $ABe_2B_3O_7$ (A = K, Rb) as UV Nonlinear Optical Crystals, *J. Am. Chem. Soc.*, 2010, **132**, 8779–8786.
14 F. Zhang, X. Chen, M. Zhang, W. Jin, S. Han, Z. Yang and S. Pan, An excellent deep-ultraviolet birefringent material based on $[BO_2]_\infty$ infinite chains, *Light: Sci. Appl.*, 2022, **11**, 252.
15 Z. Yan, D. Chu, M. Zhang, Z. Yang and S. Pan, $Li_{0.5}Na_{0.5}AlB_2O_4F_2$: Fluoroaluminoborate with Aligned $^1_\infty[BO2]$ Chain Induced by Unprecedented $[AlO_3F_3]^{6-}$ Species Features Enhanced Birefringence, *Adv. Opt. Mater.*, 2022, **11**, 2202353.
16 P. F. Li, C. L. Hu, B. X. Li, J. G. Mao and F. Kong, $Hg_3Se(SeO_3)(SO_4)$: A Mixed-Valent Selenium Compound with Mid-Infrared Transmittance Obtained by In Situ Reaction, *Inorg. Chem.*, 2024, **63**, 4011–4016.
17 J. R. Lv, G. J. Yi, X. Zou, H. K. Liu, X. Y. Han, L. Huang, H. M. Zeng, Z. Lin and G. H. Zou, Birefringence Disparity Induced by Synergistic Effects of Stereochemically Active Lone Pairs, *Chem. Mater.*, 2024, **36**, 12018–12025.
18 Y. Deng, L. Huang, X. Dong, L. Wang, K. M. Ok, H. Zeng, Z. Lin and G. Zou, $K_2Sb(P_2O_7)F$: Cairo Pentagonal Layer with Bifunctional Genes Reveal Optical Performance, *Angew. Chem., Int. Ed.*, 2020, **59**, 21151–21156.
19 X. Zhou, X. Mao, P. Zhang, X. Dong, L. Huang, L. Cao, D. Gao and G. Zou, Designing excellent UV birefringent materials through the synergistic interaction of two highly distorted functional groups, *Inorg. Chem. Front.*, 2024, **11**, 3221–3228.
20 P. F. Li, C. L. Hu, Y. F. Li, J. G. Mao and F. Kong, $Hg_4(Te_2O_5)(SO_4)$: A Giant Birefringent Sulfate Crystal Triggered by a Highly Selective Cation, *J. Am. Chem. Soc.*, 2024, **146**, 7868–7874.
21 C. Wu, X. Jiang, Z. Wang, L. Lin, Z. Lin, Z. Huang, X. Long, M. G. Humphrey and C. Zhang, Giant Optical Anisotropy in the UV-Transparent 2D Nonlinear Optical Material $Sc(IO_3)_2(NO_3)$, *Angew. Chem., Int. Ed.*, 2021, **60**, 3464–3468.
22 B. Zhang, C. L. Hu, J. G. Mao and F. Kong, Fully tricoordinated assembly unveils a pioneering nonlinear optical crystal $(SbTeO_3)(NO_3)$, *Chem. Sci.*, 2024, **15**, 18549–18556.
23 F. Kong, S. P. Huang, Z. M. Sun, J. G. Mao and W. D. Cheng, $Se_2(B_2O_7)$: A New Type of Second-Order NLO Material, *J. Am. Chem. Soc.*, 2006, **128**, 7750–7751.
24 J. H. Zhang, F. Kong, B. P. Yang and J. G. Mao, A series of boroselenite-based open frameworks mediated by the cationic sizes of the alkali metals, *CrystEngComm*, 2012, **14**, 8727–8733.
25 M. Y. Cao, C. L. Hu, F. Kong, Z. Y. Xiong and J. G. Mao, $M(B(SeO_3)_3)H_2O$ (M = Al, Ga): the first boroselenites with a unique sandwich like double-layer structure, *Dalton Trans.*, 2021, **50**, 15057–15061.
26 M. Xia, X. Jiang, Z. Lin and R. Li, "All-Three-in-One": A New Bismuth-Tellurium-Borate Bi_3TeBO_9 Exhibiting Strong Second Harmonic Generation Response, *J. Am. Chem. Soc.*, 2016, **138**, 14190–14193.
27 L. Liu, J. Young, M. Smeu and P. S. Halasyamani, $Ba_4B_8TeO_{19}$: A UV Nonlinear Optical Material, *Inorg. Chem.*, 2018, **57**, 4771–4776.
28 M. Wen, H. Wu, C. Hu, Z. Yang and S. Pan, Experiment and First-Principles Calculations of $A_2Mg_2TeB_2O_{10}$ (A = Pb, Ba): Influences of the Cosubstitution on the Structure Transformation and Optical Properties, *Inorg. Chem.*, 2019, **58**, 11127–11132.
29 R. Tang, C. Hu, J. Feng, Z. Fang, Y. Chen, F. Kong and J. Mao, $Sr_5TeO_2(BO_3)_4$ and $NaSr_5(BO_3)(SiO_4)_2$: two inorganic metal borate derivatives with diverse zero dimensional anions, *Dalton Trans.*, 2020, **49**, 3743–3749.
30 C. Zhou and R. Li, Large Difference in Nonlinear Optical Activity of Rare Earth Ion Substitution of Bi^{3+} in A_3TeBO_9 (A = Bi, La, Pr, Nd, Sm-Dy), *Inorg. Chem.*, 2023, **62**, 11265–11270.
31 J. H. Feng, C. L. Hu, X. Xu, F. Kong and J. G. Mao, $Na_2RE_2TeO_4(BO_3)_2$ (RE = Y, Dy-Lu): luminescent and structural studies on a series of mixed metal borotellurates, *Inorg. Chem.*, 2015, **54**, 2447–2454.
32 R. Ziegler, G. Heymann and H. Huppertz, Synthesis and crystal structure of the first ternary tellurium borate TeB_4O_8, *Z. Anorg. Allg. Chem.*, 2022, **648**, e202200229.
33 R. Ziegler, F. R. S. Purtscher, T. S. Hofer, G. Heymann and H. Huppertz, Single-crystal structure and theoretical calcu-

lations of the second ternary tellurium borate $Te_2B_2O_7$, *J. Solid State Chem.*, 2024, **330**, 124458.

34 J. Sun, M. Mutailipu, S. Cheng, Z. Yang and S. Pan, $Rb_3BaTeB_7O_{15}$: a novel $[B_7O_{16}]$ fundamental building block in a new telluroborate with $[TeO_3]$ polyhedra, *Dalton Trans.*, 2020, **49**, 8911–8917.

35 T. Zhang, L.-H. Deng, W.-L. Xie, C.-Y. Bai, J.-W. Feng, J.-J. Zheng and D.-H. An, $K_3BaTeB_7O_{15}$: A new borotellurite with mixed metal cations, *J. Mol. Struct.*, 2022, **1252**, 132181.

36 R. Zhang, A. Tudi, X. Yang, X. Wang, Z. Yang, S. Han and S. Pan, $PbTeB_4O_9$: a lead tellurium borate with unprecedented fundamental building block $[B_4O_{10}]$ and large birefringence, *Chem. Commun.*, 2024, **60**, 340–343.

37 J. Wang, H. Wu, H. Yu, Z. Hu, J. Wang and Y. Wu, $LaTeBO_5$: a new borotellurite with a large birefringence activated by the highly distorted $[Te^{(iv)}O_4]$ group, *Dalton Trans.*, 2021, **50**, 12404–12407.

38 M. Weil, G. Heymann and H. Huppertz, The High–Pressure Polymorph of $Ca_4Te_5O_{14}$ and the Mixed–Valent Compound $Ca_{13}TeVI_{2/3}TeIV_{3.75}O_{15}(BO_3)_4(OH)_3$, *Eur. J. Inorg. Chem.*, 2016, **2016**, 3574–3579.

39 G. M. Sheldrick, SHELXT – integrated space-group and crystal-structure determination, *Acta Crystallogr., Sect. A: Found. Adv.*, 2015, **71**, 3–8.

40 O. V. Dolomanov, L. J. Bourhis, R. J. Gildea, J. A. K. Howard and H. Puschmann, OLEX2: a complete structure solution, refinement and analysis program, *J. Appl. Crystallogr.*, 2009, **42**, 339–341.

41 G. M. Sheldrick, Crystal structure refinement with SHELXL, *Acta Crystallogr., Sect. A: Found. Adv.*, 2015, **71**, 3–8.

42 A. L. Spek, Single-crystal structure validation with the program PLATON, *J. Appl. Crystallogr.*, 2003, **36**, 7–13.

43 M. D. Segall, P. J. D. Lindan, M. J. Probert, C. J. Pickard, P. J. Hasnip, S. J. Clark and M. C. Payne, First-principles simulation: ideas, illustrations and the CASTEP code, *J. Phys.: Condens. Matter*, 2002, **14**, 2717–2744.

44 V. Milman, B. Winkler, J. A. White, C. J. Pickard, M. C. Payne, E. V. Akhmatskaya and R. H. Nobes, Electronic structure, properties, and phase stability of inorganic crystals: A pseudopotential plane-wave study, *Int. J. Quantum Chem.*, 2000, **77**, 895–910.

45 J. P. Perdew, K. Burke and M. Ernzerhof, Generalized Gradient Approximation Made Simple, *Phys. Rev. Lett.*, 1996, **77**, 3865–3868.

46 J. S. Lin, A. Qteish, M. C. Payne and V. V. Heine, Optimized and transferable nonlocal separable ab initio pseudopotentials, *Phys. Rev. B: Condens. Matter Mater. Phys.*, 1993, **47**, 4174–4180.

47 M. J. Frisch, G. W. Trucks and H. B. Schlegel, *Gaussian 09, Revision A 02*, Wallingford CT, 2009.

48 T. Lu and F. Chen, Multiwfn: a multifunctional wavefunction analyzer, *J. Comput. Chem.*, 2012, **33**, 580–592.

49 X. Shi, A. Tudi, M. Cheng, F. Zhang, Z. Yang, S. Han and S. Pan, Noncentrosymmetric Rare-Earth Borate Fluoride $La_2B_5O_9F_3$: A New Ultraviolet Nonlinear Optical Crystal with Enhanced Linear and Nonlinear Performance, *ACS Appl. Mater. Interfaces*, 2022, **14**, 18704–18712.

50 R. L. Tang, Y. L. Wei, Y. Chi, Z. H. Shi, W. Liu and S. P. Guo, Cation Regulation to Investigate the Chalcogenide Borate $RE_6Nb_2MgSB_8O_{26}$ (RE = La-Nd) Family, *Inorg. Chem.*, 2022, **61**, 8653–8661.

51 X. Long, R. An, Y. Lv, X. Wu and M. Mutailipu, Tunable Optical Anisotropy in Rare-Earth Borates with Flexible $[BO_3]$ Clusters, *Chem. – Eur. J.*, 2024, **30**, e202401488.

52 J. Lin, K. Diefenbach, M. A. Silver, N. S. Dalal and T. E. Albrecht-Schmitt, Structure–Property Correlations in the Heterobimetallic 4f/3d Materials $Ln_2M(TeO_3)_2(SO_4)$ (Ln = Y, Nd, Sm, Eu, Gd, Tb, Dy, Ho, Er, Tm, Yb, or Lu; M = Co or Zn), *Cryst. Growth Des.*, 2015, **15**, 4606–4615.

53 H. E. Lee, H. Jo, M. H. Lee and K. M. Ok, Unique synthesis, structure determination, and optical properties of seven new layered rare earth tellurite nitrates, $RE(TeO_3)(NO_3)$ (RE = La, Nd, Eu, Gd, Dy, Er, and Y), *J. Alloys Compd.*, 2021, **851**, 156855.

54 P. F. Chen, C. L. Hu, M. Y. Cao, X. Y. Zhang and J. G. Mao, $AKTeO_2(CO_3)$ (A = Li, Na): The First Carbonatotellurites Featuring a Zero-Dimensional $[Te_2C_2O_{10}]^{4-}$ Cluster and a Wide Band Gap, *Inorg. Chem.*, 2023, **62**, 6864–6870.

55 L. P. Wang, D. T. Tu, C. L. Li, S. Y. Han, F. Wen, S. Q. Yu, X. D. Yi, Z. Xie and X. Y. Chen, Engineering trap distribution to achieve multicolor persistent and photostimulated luminescence from ultraviolet to near-infrared II, *Matter*, 2023, **6**, 4261–4273.

56 Y. Liu, X. Rong, M. Li, M. S. Molokeev, J. Zhao and Z. Xia, Incorporating Rare-Earth Terbium(III) Ions into $Cs_2AgInCl_6$: Bi Nanocrystals toward Tunable Photoluminescence, *Angew. Chem., Int. Ed.*, 2020, **59**, 11634–11640.

57 Z. Wang, Y. Wei, C. Liu, Y. Liu and M. Hong, Mn^{2+}–Activated $Cs_3Cu_2I_5$ Nano–Scintillators for Ultra–High Resolution Flexible X–Ray Imaging, *Laser Photonics Rev.*, 2023, **17**, 2200851.

58 X. Chen, B. Zhang, F. Zhang, Y. Wang, M. Zhang, Z. Yang, K. R. Poeppelmeier and S. Pan, Designing an Excellent Deep-Ultraviolet Birefringent Material for Light Polarization, *J. Am. Chem. Soc.*, 2018, **140**, 16311–16319.

59 W. Zhang, Z. He, C. Qiu, M. Cui, Z. Zhao and S. Chen, Structure and magnetism of novel mixed-anionic-group compounds $M_2(SeO_3)(Te_3O_7)$ ($M = Co^{2+}$, Ni^{2+}), *J. Alloys Compd.*, 2017, **728**, 253–258.

60 J. Lin, P. Chai, K. Diefenbach, M. Shatruk and T. E. Albrecht-Schmitt, Challenges in the Search for Magnetic Coupling in 3d/4f Materials: Syntheses, Structures, and Magnetic Properties of the Lanthanide Copper Heterobimetallic Compounds, $RE_2Cu(TeO_3)_2(SO_4)_2$, *Chem. Mater.*, 2014, **26**, 2187–2194.